Development of Superstrate CuInGaSe2 Thin Film Solar Cells with Low-Cost Electrochemical Route from Nonaqueous Bath

Article *in* ACS Sustainable Chemistry & Engineering · February 2018

DOI: 10.1021/acssuschemeng.7b04615

CITATIONS
0

READS
171

5 authors, including:

Priyanka Londhe
Savitribai Phule Pune University
27 PUBLICATIONS **62** CITATIONS
SEE PROFILE

Ashwini Rohom
Savitribai Phule Pune University
26 PUBLICATIONS **46** CITATIONS
SEE PROFILE

Rohan Fernandes
Università degli Studi di Trento
56 PUBLICATIONS **1,407** CITATIONS
SEE PROFILE

D C Kothari
University of Mumbai
183 PUBLICATIONS **1,704** CITATIONS
SEE PROFILE

ACS Sustainable Chemistry & Engineering

Research Article

Cite This: ACS Sustainable Chem. Eng. XXXX, XXX, XXX−XXX

pubs.acs.org/journal/ascecg

Development of Superstrate $CuInGaSe_2$ Thin Film Solar Cells with Low-Cost Electrochemical Route from Nonaqueous Bath

Priyanka U. Londhe,[†] Ashwini B. Rohom,[†] Rohan Fernandes,[‡] D. C. Kothari,[‡] and Nandu B. Chaure*[,†]

[†]Department of Physics, Savitribai Phule Pune University (formerly University of Pune), Pune 411007, India

[‡]Department of Physics and National Centre for Nanosciences & Nanotechnology, University of Mumbai, Vidyanagri, Santacruz (E), Mumbai 400098, India

Supporting Information

ABSTRACT: Electrodeposition of $Cu(In,Ga)Se_2$ (CIGS) thin film is an attractive approach for the development of highly efficient low-cost solar cells. This work focuses on the effects of various electrodeposition parameters on the growth and properties of CIGS layers. The films deposited at −0.9 V tend to drive the growth of CIGS favoring (112) crystal orientation, whereas the films deposited at −1.6 V show the orientation along (220)/(204). Interplanar distances corresponding to (112) and (204/220) planes could be observed in the high resolution transmission electron microscopy (HRTEM) images of the respective films, confirming the dependence of the texture on the deposition potential. Films with larger grains could be grown by maintaining higher temperature (130 °C) during the deposition of layers. X-ray photoelectron spectroscopy (XPS) confirmed the presence of Cu^+, In^{3+}, Ga^{3+}, and Se^{2-} valence states in the CIGS layers prepared at −0.9 and −1.6 V. The film deposited at −1.6 V with (220/204) orientation showed high efficiency as compared to the film deposited at −0.9 V with (112) orientation. The observed solar cell parameters, measured under illuminated condition of input power intensity 100 mW/cm^2, were V_{OC} = 0.357 V; J_{SC} = 27 mA/cm^2, FF = 44, and η = 4.90; and V_{OC} = 0.460 V, J_{SC} = 34 mA/cm^2, FF = 58, and η = 9.07 for the deposition potentials of −0.9 and −1.6 V, respectively.

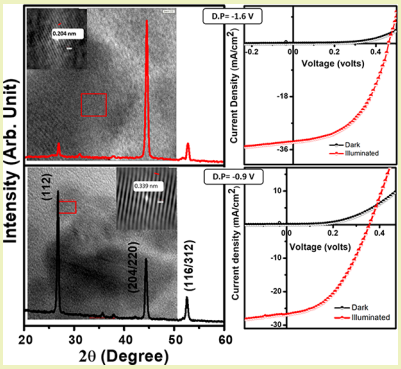

KEYWORDS: *CIGS, Low-cost electrodeposition technique, Thin film solar cells, Structural properties, Optoelectronic properties*

INTRODUCTION

Steps forward for photovoltaic (PV) technologies are necessary for the production of electrical power from renewable sources. Thin films solar cells are flourishing and anticipated to grow considerably because of their low cost and also because they offer a wide variety of choices in terms of device design and fabrication. Ternary and quaternary semiconducting compounds such as $CuInSe_2$ (CIS) and $Cu(In,Ga)Se_2$ (CIGS) have attracted considerable interests over the past few decades as fascinating absorber materials in efficient thin film solar cells (TFSC).[1−3] Due to the long-term stability, direct energy band gap with high optical absorption coefficient, and long diffusion lengths of minority carriers, CIGS is one of the most promising materials in the thin film solar cell category with a maximum reported laboratory-scale cell efficiency of ∼22.3%.[4]

Currently the efforts are ongoing to enhance the efficiency to the theoretical maximum (∼30%)[5] as well as to develop cheaper strategies for the absorber layer. To date, several solar cell technologies have been established with extraordinary energy conversion efficiencies.[6] The reported highest efficiency for CIGS is obtained by the vacuum-based coevaporation technique.[4] Numerous vacuum- and nonvacuum-based methods have been used for the deposition of CIGS layers for solar cell devices; however, the vacuum-based method creates cost and technological barriers for the production of low-cost photovoltaic modules.[7,8] Among the different nonvacuum-based methods, electrodeposition is one of the most studied techniques.[9,10] The intent of our study is to circumvent the cost-intensive vacuum-based deposition method and develop CIGS solar cells using a low-cost electrochemical method. The method has several advantages such as low instrumental and materials costs, high deposition speed, efficient utilization of raw materials, and feasibility in making large area thin films.[11] The most common approach to electrodeposit CIGS is based in aqueous solutions;[12] however, the hydrogen evolution limits the adherence and quality of thin films. Ionic liquids as a solvent are reported as alternatives to aqueous solutions to deposit CIS-based layers. Due to the hygroscopic nature of ionic liquids, a controlled atmosphere is required which confines its use.[13] The film prepared by electrodeposition requires post-heat treatment, such as annealing, selenization/sulfurization, etc. to improve the crystallinity. However, for flexible plastic substrates, the layer cannot be annealed/selenized at high temperature. To overcome these issues, nonaqueous solvents such as ethylene glycol, diethylene glycol, polyethylene glycol, etc. may be used for CIGS deposition.[14] They have several advantages such as wide electrochemical windows, high boiling points, and flexibility of selecting the

Received: December 6, 2017
Revised: January 27, 2018
Published: February 20, 2018

DOI: 10.1021/acssuschemeng.7b04615
ACS Sustainable Chem. Eng. XXXX, XXX, XXX−XXX

organic and inorganic compounds.[15] Importantly, the wide electrochemical window is available for depositing the desired contents of Ga along with Cu, In, and Se and large grain growth.

The highest reported CIGS solar cell efficiency by electrodeposition is 15%.[16] A multilayer superstrate solar cell structure was prepared by Chaure et al.[17] using an electrodeposition technique with an efficiency ∼9%.

In this paper, we present a comprehensive study on the synthesis of a CIGS layer using a low-cost electrochemical route with nonaqueous solvents and focus on studying the effects of various electrodeposition parameters on the growth and properties of CIGS layers. The superstrate solar cells of a Glass/FTO/CdS/CIGS structure, prepared using CIGS grown at different potentials, are characterized for structural and optoelectronic properties.

MATERIALS AND METHODS

Sample Preparation. One-step electrodeposition from a nonaqueous medium (ethylene glycol) was employed for the deposition of CIGS samples. The CIGS layers were deposited potentiostatically onto fluorine-doped tin oxide (FTO)-coated glass substrates at 130 °C using a Bio-Logic potentiostat/galvanostat model SP150.

To understand the electrochemical mechanism of CIGS growth in ethylene glycol (EG), electrochemistry of a Cu−In−Ga−Se system was studied using cyclic voltammetry (CV). The bath matrix consisted of copper(II) chloride ($CuCl_2$), indium chloride ($InCl_3$), selenium tetrachloride ($SeCl_4$), and gallium chloride ($GaCl_3$). LiCl was used as a supporting chemical compound to control ionic conductivity of the bath. A standard three-electrode geometry with Ag/AgCl as the reference electrode, FTO as the working electrode, and graphite as the counter electrode was used. CV measurements and deposition of CIGS layers were performed without agitation at 130 °C. The potentials −0.9 and −1.6 V versus Ag/AgCl were optimized from CV measurements for the electrodeposition of CIGS. CIGS samples were annealed with selenium ambient in a tubular furnace at 400 °C for 20 min. A graphite box consisting of CIGS layers and Se ingots was placed in the quartz tube with a vacuum of $\sim 5 \times 10^{-2}$ Torr. The annealing was carried out in two-steps, initially the whole assembly was heated at 200 °C for 15 min, and subsequently, the temperature was increased to 400 °C with a heating rate of 50 °C/sec. The samples were cooled to room temperature naturally. Solar cell devices were prepared in a superstrate FTO/CdS/CIGS/Au solar cell structure, wherein CIGS layers were electrodeposited at −0.9 or −1.6 V. CdS layers were prepared by a chemical bath deposition technique[18] to complete the final superstrate FTO/CdS/CIGS/Au solar cell structure. Au-metal contact of a diameter of 2 mm was made by a thermal evaporation technique at a vacuum of $\sim 10^{-6}$ mbar. Prior to the Au-metal contact, CdS/CIGS layers were etched in Br_2/methanol and NaCN solutions for 30 s each.

Characterization Techniques. Cyclic voltammetry (CV) measurements were performed using a Bio-Logic potentiostat/galvanostat model SP 150. The as-deposited and selenized layers grown at different potentials were characterized for structural and compositional properties. The structural properties were studied by means of an X-ray diffractometer (XRD), model Bruker D8 with Cu Kα radiation of wavelength 1.5405 Å, and transmission electron microscopy (TEM) model TECNAI G2. The surface topography was examined using a JEOL J SPM-5200 scanning probe microscope (SPM). The bulk elemental atomic percentage concentration was determined by an energy dispersive X-ray analysis technique equipped in the SEM unit. The wavelength dispersive Philips PW2440 sequential X-ray fluorescence spectrometer was used to determine the elemental concentrations of CIGS layers. The surface composition and chemical states of each element were examined by X-ray photoelectron spectra (XPS) using a PHI 5000 VersaProbe II instrument equipped with a monochromatic Al Kα (1486.6 eV) X-ray source and a hemispherical analyzer. Appropriate electrical charge compensation was employed to perform the analysis, and binding energy was referenced to the C 1s peak at 284.8 eV. The final solar cell devices were measured for solar cell parameters in dark and illuminated conditions at room temperatures. For the visible light illumination, an input power intensity of 100 mW/cm^2 (1.5 AM) was used. External quantum efficiency (EQE) was measured by a photon counting spectrometer, ISS Inc., and Kiethley 2400 source meter.

RESULTS AND DISCUSSION

Cyclic Voltammetry Measurements. In order to achieve prologue information about electrochemical behavior and reduction of CIGS, a cyclic voltammogram for the quaternary Cu−In−Ga−Se system prepared on FTO glass was recorded. Figure 1 shows typical the cyclic voltammograms recorded for the quaternary Cu−In−Ga−Se system at a scan rate of 10 mV/s.

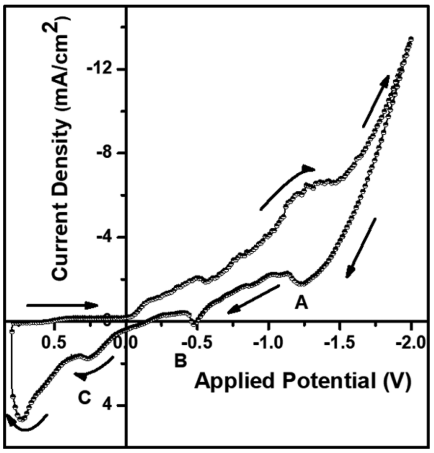

Figure 1. Typical cyclic voltammogram recorded in electrolyte consisting of ionic species $CuCl_2$, $InCl_3$, $GaCl_3$, and $SeCl_4$, with scan rate 10 mV/s at temperature of 130 °C using Ag/AgCl reference electrode on FTO substrate.

A cathodic current starts to increase at the beginning of a forward scan at about +0.52 V followed by a plateau region in the range from +0.52 V to −0.05 V. This plateau corresponds to the reduction of ionic copper species to copper by the following charge transfer reactions:

$$Cu^{2+} + 2e^- \rightarrow Cu \quad E_0 = +0.34\ \text{V vs SCE} \tag{1}$$

$$Cu^{2+} + e^- \rightarrow Cu^+ \quad E_0 = +0.16\ \text{V vs SCE} \tag{2}$$

$$Cu^+ + e^- \rightarrow Cu \quad E_0 = +0.52\ \text{V vs SCE} \tag{3}$$

A slight increase in current seen at about −0.5 V is proposed to be due to the reaction of selenium by the following charge transfer reaction:

$$Se^{4+} + 6e^- \rightarrow Se^{2-} \quad E_0 = +0.048\ \text{V vs SCE} \tag{4}$$

The reduction peaks observed at about −0.17 and −0.51 V are proposed to be due to the reduction of In^{3+} to In and Ga^{3+} to Ga according to charge transfer reactions (5) and (6):

$$In^{3+} + 3e^- \rightarrow In \quad E_0 = -0.34\ \text{V vs SCE} \tag{5}$$

$$Ga^{3+} + e^- \rightarrow Ga \quad E_0 = -0.56\ \text{V vs SCE} \tag{6}$$

Further linear rise in the cathodic current after −0.65 V with increasing the cathodic potential may be due to the deposition

DOI: 10.1021/acssuschemeng.7b04615
ACS Sustainable Chem. Eng. XXXX, XXX, XXX−XXX

of Ga and In along with Cu and Se. The cathodic current is found to be increased beyond −1.0 V, which may be due to the co-deposition of Cu, In, Ga, and Se. We have not observed any bubbling from the cathode at higher cathodic potentials, which confirms the absence of hydrogen evolution. The peaks observed during the anodic scan marked as A, B, and C are due to the stripping of In, Se, and Cu, respectively.

Structural Study. Figure 2 depicts the X-ray diffractograms of typical as-grown CIGS layers at −0.9 and −1.6 V. XRD patterns exhibit three prominent reflectionns (112), (204/220), and (312)/(116) that correspond to the chalcopyrite crystal structure of CIGS. It is noteworthy that the as-deposited layers prepared at −0.9 and −1.6 V exhibit (112) and (204/220) textures, respectively. The secondary binary phases, Cu_2Se and In_2Se_3, indicated in the XRD patterns shown in Figure 2 are attributed to the applied potentials −0.9 and −1.6 V, respectively. As per the equilibrium potentials (reactions 1 and 5), Cu-rich and In-rich layers are expected for lower (−0.9 V) and higher (−1.6 V) growth potentials, respectively.

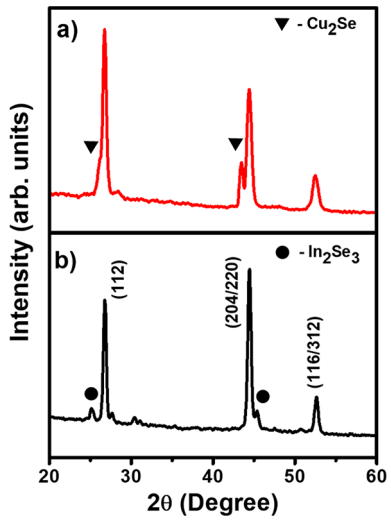

Figure 2. X-ray diffractograms of the as-deposited CIGS thin film deposited at (a) −0.9 V and (b) −1.6 V with respect to Ag/AgCl reference electrode.

The XRD pattern of the annealed layers is shown in Figure 3. The peaks of the chalcopyrite structure of CIGS observed at 2θ = 26.76°, 44.47°, and 52.47° correspond to (112), (220/204), and (312) planes, respectively(JCPDS data Card No. = 35-1102). The annealed layer deposited at −0.9 V exhibits strong (112) orientation, whereas the strong (220/204) orientation can be clearly seen in Figure 3b. The preferential orientation was further confirmed by HRTEM as shown adjacent to the respective XRD patterns. The values of interplanar distance, 0.204 and 0.339 nm, obtained for the annealed CIGS sample prepared at −0.9 and −1.6 V correspond to (112) and (220)/(204) reflections, respectively. Several reports are available on the studies of orientation of CIGS thin films prepared by the co-evaporation and sputtering technique; however, to the authors' best knowledge, the control of orientation achieved by varying the electrodeposition process parameters has not been reported so far. The most stable and favorable preferred orientation of the CIGS is of the (112) plane, which is parallel to the substrate orientation as experimentally reported[19,20] as well as theoretically predicted.[21] However, achieving [220]/[204] orientation is challenging. Schlenker et al.[22] reported the substrate effects on the texture orientation. Contreras et al.[23] accounted that the preferential orientation of CIGS can be changed by varying the crystallographic orientation of the $(In,Ga)_2Se_3$ layer by the three-stage co-evaporation process. Nonetheless, Contreras et al.[24] also report that other parameters also influence the film orientation. They particularly highlighted the effect of nature of the glass substrate for the (220)/(204) orientation, which may get prompted by the diffusion of sodium into the growing CIGS layer from the substrate. Wallin et al.[25] and Hanna et al.[26] proposed that the growth of an absorber layer deposited under Se-rich conditions helps in growing the (220)/(204)-oriented layer. Contreras et al.[27] observed increased device performance with higher Se flux driven by an increase in open circuit voltage as well as the fill factor, whereas Yun et al.[28] found that an intermediate Se

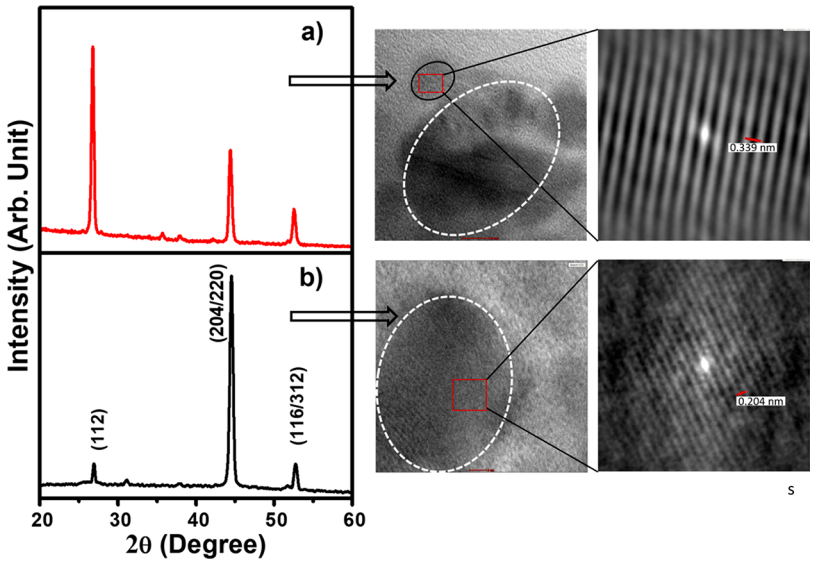

Figure 3. X-ray diffractogram of the annealed CIGS thin film deposited at (a) −0.9 V and (b) −1.6 V. Adjacent images corresponds HRTEM of the respective sample.

DOI: 10.1021/acssuschemeng.7b04615
ACS Sustainable Chem. Eng. XXXX, XXX, XXX−XXX

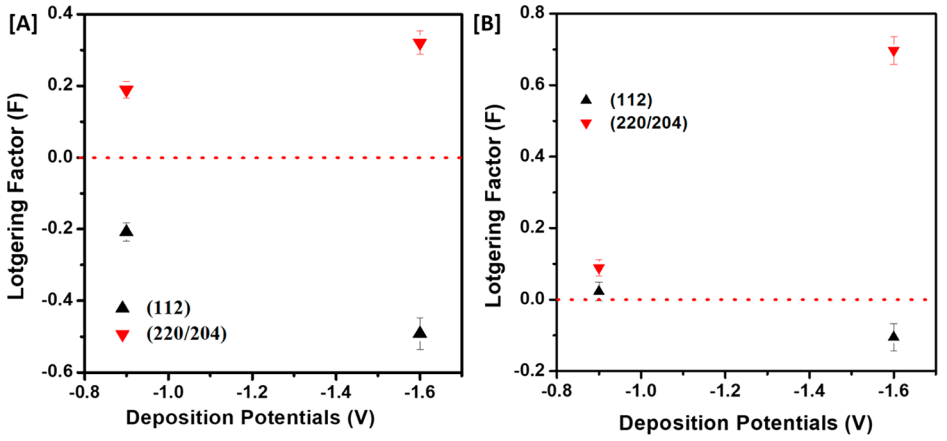

Figure 4. Variation of Lotgering factor (F) as a function of deposition potential for (A) as-deposited and (B) annealed CIGS thin film.

Table 1. Summary of Compositional analysis of $CuInGaSe_2$ Thin Films Electrodeposited at −0.9 and −1.6 V Determined by EDAX and XRF

	Atomic Composition (%)									
	Cu		In		Ga		Se		Ga/(In+Ga)	
Deposition Potential (V)	EDAX	XRF	EDAX	XRF	EDAX	XRF	EDAX	XRF	EDAX	XRF
−0.9	21.23	22.00	22.48	21.00	03.00	02.90	53.29	54.10	0.12	0.12
−1.6	10.74	12.50	33.07	30.00	06.02	06.50	50.17	51.00	0.16	0.18

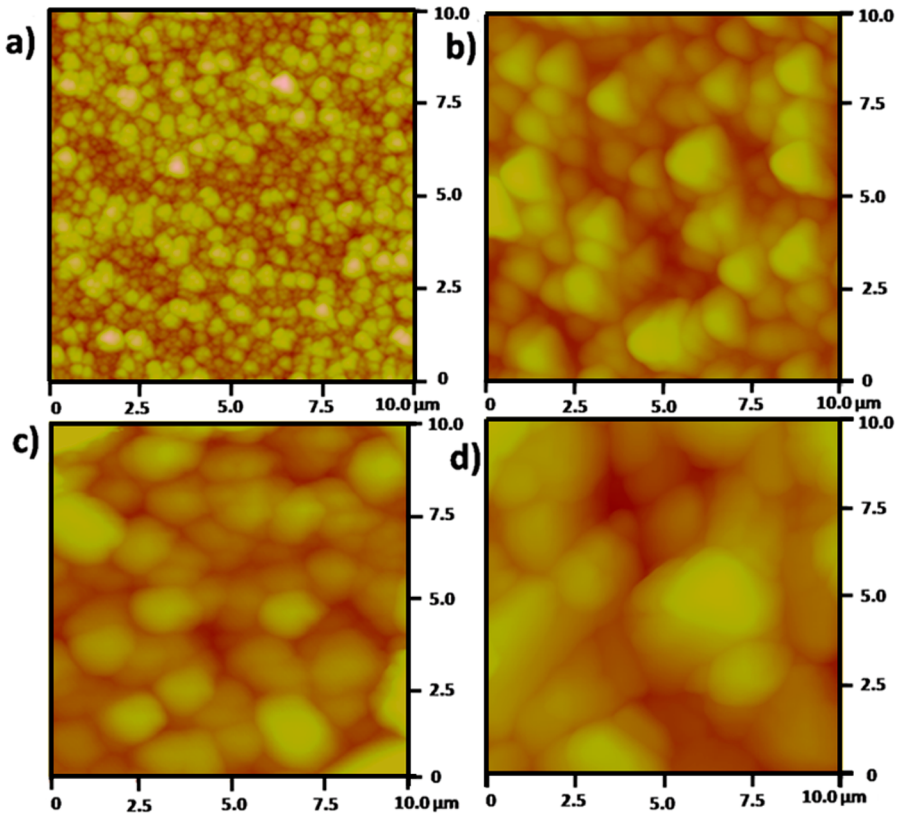

Figure 5. AFM images of (a, c) as-deposited and (b, d) annealed CIGS thin films deposited at −0.9 and −1.6 V, respectively.

evaporation rate was optimal. In our case, the observed preferential (220)/(204) texture for the CIGS film deposited at −1.6 V could be due to the formation of the In_2Se_3 phase along with CIGS in an as-deposited sample and also the growth of a copper-poor layer. It has been reported in the literature that the $In_2Se_3/(In,Ga)_2Se_3$ layer helps in growing the CIGS layer with a (220/204) orientation.[23,29,30]

The preferred orientations of the CIGS films were obtained with Lotgering factors. The reflections as a function of deposition potential for the as-deposited and annealed layers are shown in Figure 4(A) and (B), respectively.

DOI: 10.1021/acssuschemeng.7b04615
ACS Sustainable Chem. Eng. XXXX, XXX, XXX−XXX

The Lotgering factor is given by following relation:[31]

$$F_{\langle 00l \rangle} = \frac{\frac{\sum I_{\{00l\}}}{\sum I_{\{hkl\}}} - \frac{\sum I_{0\{00l\}}}{\sum I_{0\{hkl\}}}}{1 - \frac{\sum I_{0\{00l\}}}{\sum I_{0\{hkl\}}}} \quad (7)$$

where I and I_0 are the peak intensities of the textured and randomly oriented sample, respectively. Positive values of the Lotgering factor designates that the surface orientation (hkl) is prominent, whereas a negative value implies a reduced occurrence of the (hkl) orientation. It is clearly obvious from Figure 4 that the as-prepared and annealed CIGS layers deposited at −1.6 V exhibits a (220)/(204) preferred orientation.

The compositional analysis of annealed CIGS thin films deposited at −0.9 and −1.6 V were obtained by energy dispersive analysis of X-rays (EDAX), and the results are summarized in Table 1. We have further determined the elemental percentage concentration of all the CIGS layers deposited for potentials ranging from −0.8 to −1.6 V by XRF, and the results are given in the Supporting Information (Figure S1).

Cu deficient layers were obtained at −1.6 V; however, nearly stoichiometric growth with ∼3% Ga was detected for the layer grown at −0.9 V. The Ga/(Ga+In) ratio was systematically increased from 0.12 to 0.16 with increasing the growth potential.

AFM Study. Surface morphology of CIGS thin films was studied using AFM analysis. 2-D AFM images of as-deposited and annealed CIGS thin films electrodeposited at −0.9 and −1.6 V are shown in Figure 5. During electrodeposition, various parameters responsible for grain formation are bath temperature, viscosity of electrolyte, chemical concentration, and geometry of the electrode. The formation of large grains in as-deposited samples prepared at −0.9 and −1.6 V could be due to the higher working temperature (130 °C) during deposition. It is found that the film deposited at −1.6 V forms larger grains as compared to the layer deposited at −0.9 V. At higher deposition potentials, the current density is higher, leading to more driving force to nucleate but not sufficient time to grow which will result in finer grains.

The CIGS layers grown at −0.9 and −1.6 V have grain sizes approximately from 0.5 to 1.0 μm and 2.5 to 3 μm, respectively. Upon annealing, both layers became more compact, smooth, and uniform with grain sizes from ∼2 to 3 μm and 3.5 to 4.5 μm for the samples deposited at −0.9 and −1.6 V, respectively. Such a uniform and smooth film having larger grains is most suitable for charge transport in solar cell devices The root-mean-square (RMS) surface roughness calculated for the CIGS film deposited at −0.9 and −1.6 V was 15.33 and 26.53 nm for the as-deposited samples; it was 30.34 and 42.59 nm for the annealed samples, respectively. Figure 6 shows the SEM cross-section of the FTO/CdS/CIGS superstrate structure grown at −1.6 V. The thickness measured for the CIGS layer on CdS was ∼2.8 μm (±70 nm), which is very similar to the thickness measured by using a Filmetrics F10 thin film analyzer.

XPS Study. The chemical states of various elements present in the annealed CIGS thin films electrodeposited at −0.9 and −1.6 V were examined by XPS analysis. Figure 7 shows the survey spectra obtained for annealed CIGS layers deposited at −0.9 and −1.6 V.

Prior to the XPS measurement, the samples were etched in Br_2/methanol and NaCN solutions for desired conditions used

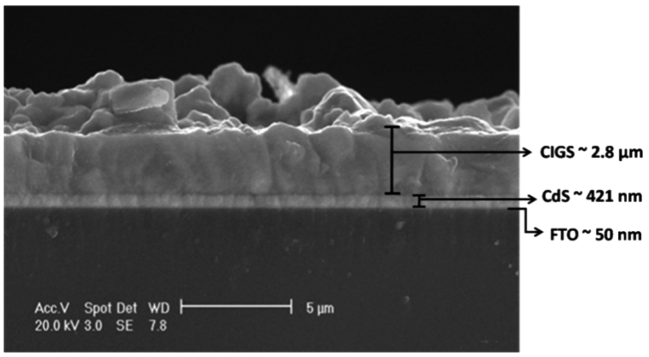

Figure 6. Typical cross-section image of FTO/CdS/CIGS (electrodeposited at −1.6 V) versus Ag/AgCl reference electrode.

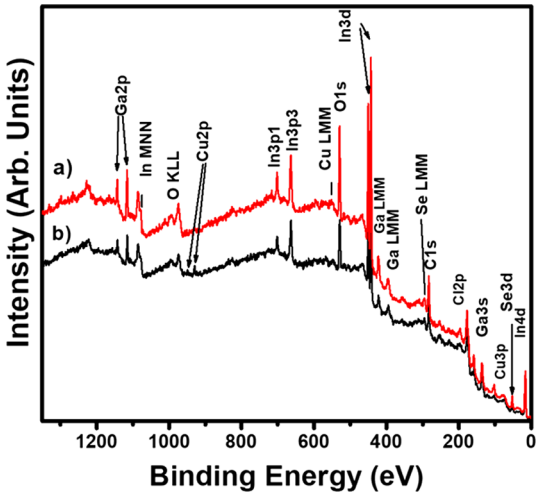

Figure 7. XPS survey spectra of annealed CIGS thin films deposited at (a) −0.9 V and (b) −1.6 V.

for the development of the final solar cell device. Along with the peak corresponds to Cu, In, Ga, and Se precursors, C 1s- and O 1s-related peaks are also exhibited in the survey scan, which could be due to the surface contamination caused by ambient conditions in the vacuum chamber. The sample grown at −0.9 V measured a higher intensity Cu signal as compared to the sample −1.6 V, which demonstrates the Cu-rich layer grown at −0.9 V. The less intense Cu peak observed for the sample grown at −1.6 V confirms that the Cu-deficient surface can form the n-type ordered defect compound (ODC) by making a homojunction within CIGS, which improves the efficiency of the solar cell. The core level spectra of Cu 2p, Ga 2p, In 3d, and Se 3d for both samples are depicted in Figure 8, and the corresponding binding energies are listed in Table 2. The obtained results are in good agreement with the reported binding energies by Lincot et al. and Calderon et al. for CIGS samples grown by the evaporation technique.[32,33]

Optoelectronic Study. The optoelectronic properties of a CdS/CIGS solar cell wherein CIGS layers were electrodeposited at −0.9 and −1.6 V have been studied. The dark and illuminated J−V curves of CdS/CIGS solar cells prepared at −0.9 and −1.6 V are depicted in Figure 9(a) and (b), respectively. The values of four basic solar cell parameters, short circuit current (J_{sc}), open circuit voltage (V_{oc}), fill factor (FF), and power conversion efficiency (η) are summarized in Table 3. In the CdS/CIGS solar cell, the CIGS layer electrodeposited at

DOI: 10.1021/acssuschemeng.7b04615
ACS Sustainable Chem. Eng. XXXX, XXX, XXX−XXX

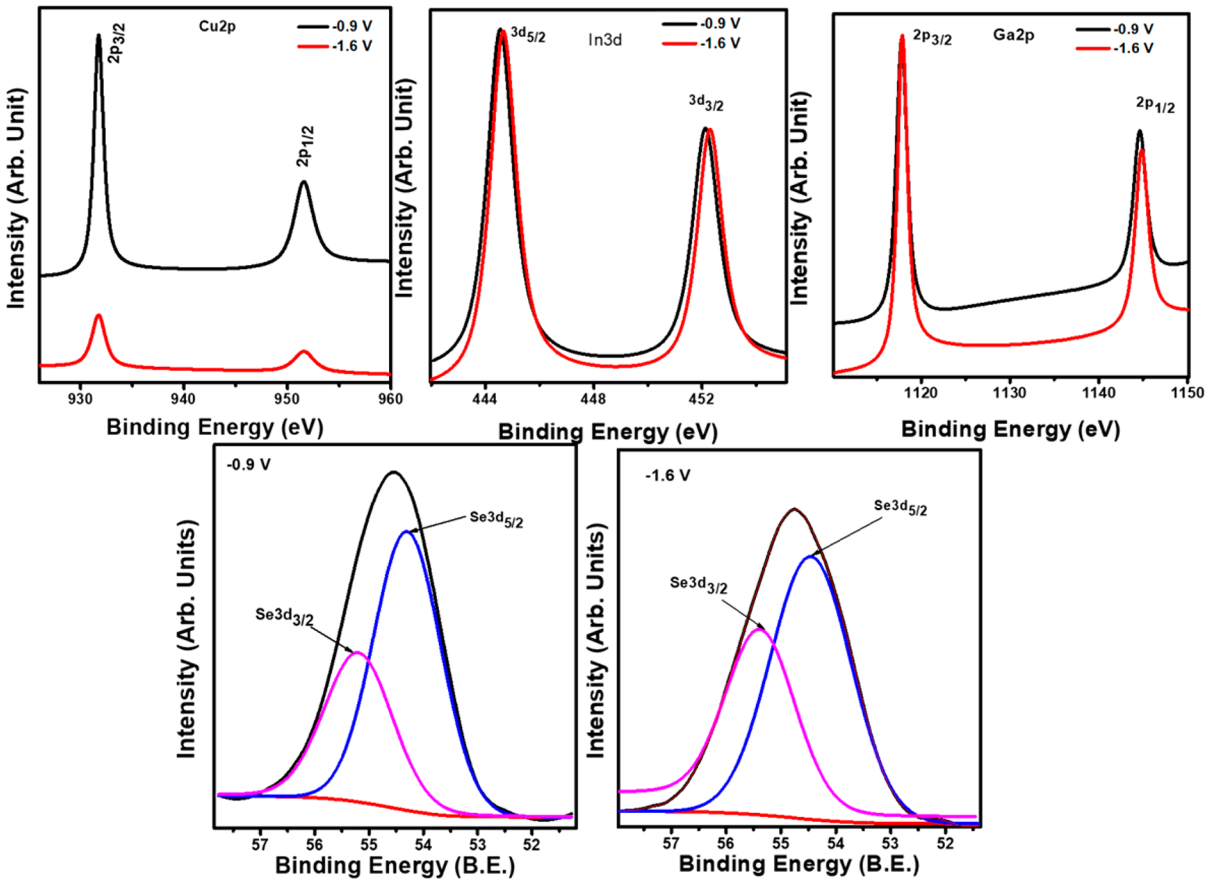

Figure 8. XPS core level spectra of annealed CIGS thin films deposited at −0.9 and −1.6 V.

Table 2. Summary of Binding Energy Peaks for Cu 2p, Ga 2p, In 3d, and Se 3d in CIGS Layers

	Binding Energies (eV)							
Deposition Potential (V)	Cu $2p_{1/2}$	Cu $2p_{3/2}$	In $3d_{3/2}$	In $3d_{5/2}$	Ga $2p_{1/2}$	Ga $2p_{3/2}$	Se $3d_{3/2}$	Se3 $d_{5/2}$
−0.9	951.5	931.7	452.1	444.5	1144.6	1117.8	55.0	54.2
−1.6	951.5	931.7	452.3	444.6	1144.9	1117.9	55.5	54.5

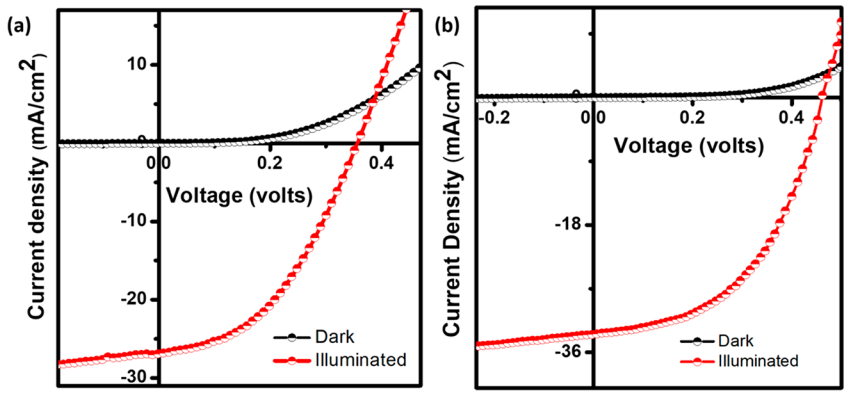

Figure 9. Dark and illuminated J−V curves of CdS/CIGS heterostructure solar cell device. CIGS layer was electrodeposited at (a) −0.9 V and (b) −1.6 V versus Ag/AgCl reference electrode.

Table 3. Solar Cell Parameters Obtained under Dark and Illuminated Conditions

Cell	V_{OC} (volts)	J_{SC} (mA/cm^2)	FF	η (%)	G_D (mS/cm^2)	G_L (mS/cm^2)	$R_{S,D}$ (Ω cm^2)	$R_{S,L}$ (Ω cm^2)	A_D	A_L
FTO/CdS/CIGS(−0.9 V)/Au	0.357	27	0.44	4.90	0.9	07	16	4.3	2.2	1.7
FTO/CdS/CIGS(−1.6 V)/Au	0.460	34	0.58	9.07	1.5	13	21	2.0	1.9	1.5

DOI: 10.1021/acssuschemeng.7b04615
ACS Sustainable Chem. Eng. XXXX, XXX, XXX−XXX

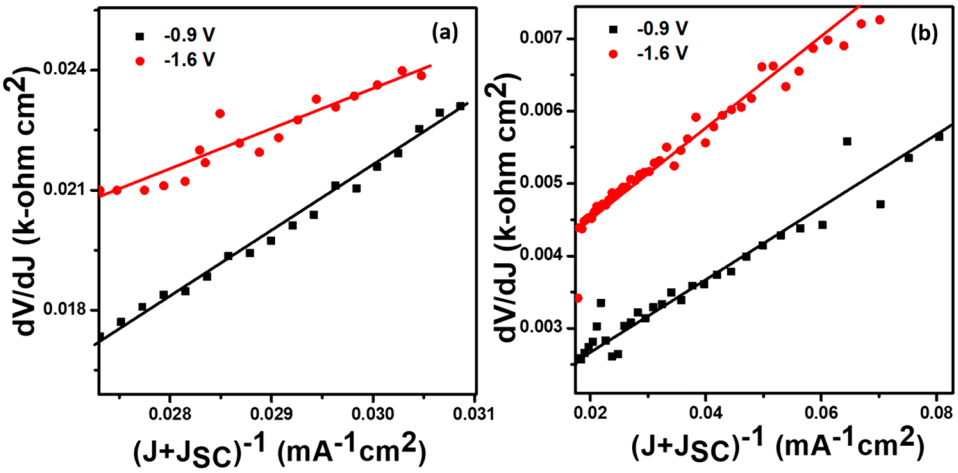

Figure 10. Graph of dV/dJ vs $(J + J_{SC})^{-1}$ for CdS/CIGS solar measured in (a) dark and (b) illuminated conditions for the film electrodeposited at −0.9 V and (c) dark and (d) illuminated conditions for the film electrodeposited at −1.6 V. The experimental data depicted in Figure 9 is processed to obtain these graphs.

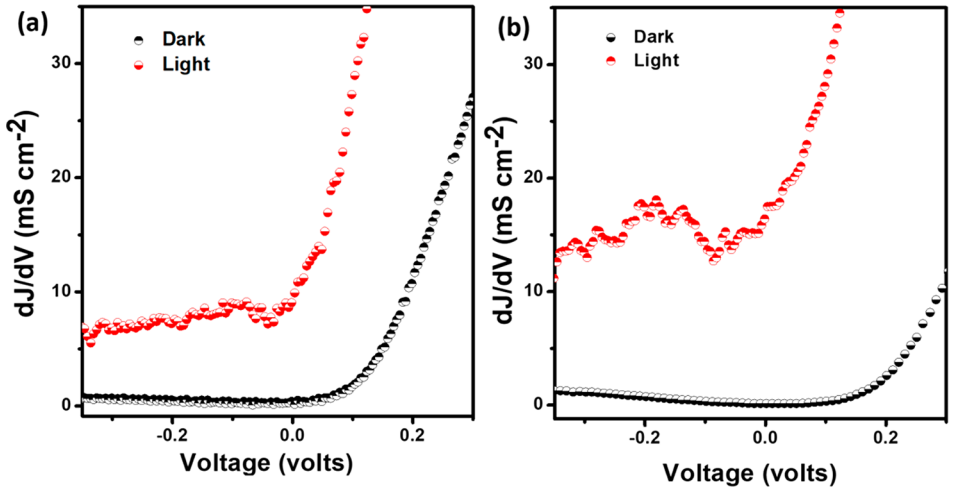

Figure 11. Graphs of dJ/dV vs V for CdS/CIGS heterostructure solar cell device. CIGS layer was electrodeposited at (a) −0.9 V and (b) −1.6 V. The experimental data depicted in Figure 9 is processed to obtain these graphs.

−1.6 V shows better solar cell parameters as compared to the layer deposited at −0.9 V.

The following general diode eq 8 was used to obtain the series resistance, shunt conductance and ideality factor.

$$J = J_0 \exp\left[\frac{q}{nkT}(V - RJ)\right] + GV - J_L \quad (8)$$

where R and G are the series resistance and shunt conductance, which arise in series and parallel with the device, respectively.

The values of the series resistance and ideality factor are estimated from the plots dJ/dV versus V and dV/dJ versus $(J + J_{sc})^{-1}$ by using the J−V curves in dark and illuminated conditions. Figure 10 illustrate the plots of dV/dJ versus $(J + J_{sc})^{-1}$ for the CIGS layer deposited at −0.9 and −1.6 V in dark and illuminated conditions, respectively.

The diode term in eq 8 becomes negligible for the plot dJ/dV against V (Figure 11) near J_{sc} and in reverse bias.

The values of shunt conductance ($G_{D,L}$), series resistance ($R_{S,D,L}$), and ideality factor ($A_{D,L}$) for both the cells under dark and illuminated conditions are tabulated in Table 3. The value of shunt conductance is found to be increased and series resistance value decreased for the solar cell prepared at −1.6 V. Thus, the film having (220/204) orientation shows higher efficiency as compared to the (112)-orientated film. Larger grain size, witnessed in the film deposited at higher cathodic potential, helps in achieving better solar cell properties. The defect states present in the absorber layer or at the interface or in the CdS layer are mainly contributed to the crossover observed in both J−V curves. This may be due to the presence of defect states in the absorber or at the heterointerface or in the CdS layer.[34−36]

The increased efficiency measured for the cell grown at −1.6 V was further confirmed by external quantum efficiency (EQE) measurements. Figure 12 depicts the EQE curves measured for the cell grown at −1.6 and −0.9 V potentials. Both cells revealed a high response to the visible region (450−800 nm). However, the spectrum for the cell deposited at higher deposition potential shows a slight blue shift of the onset wavelength due to the increased band edge transition.

The external quantum efficiency for the device fabricated using the CIGS layer grown at −1.6 V was found to be increased in the region from ∼750 to 950 nm as compared to −0.9 V and could be due to the thickness of the CIGS layer and the trap state present in the bulk CIGS. The trap states leads to

DOI: 10.1021/acssuschemeng.7b04615
ACS Sustainable Chem. Eng. XXXX, XXX, XXX−XXX

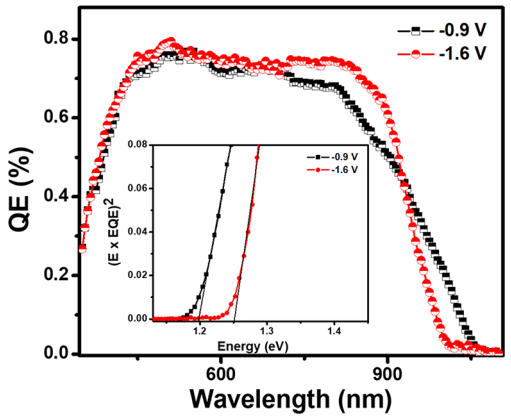

Figure 12. External quantum efficiency (EQE) curve for FTO/CdS/CIGS/Au superstrate solar cell structure. Inset shows the graph for energy band gap determination.

the recombination of electrons and holes, whereas thickness directly affects the absorption of light. The band gap of the CIGS layer is determined from a plot of $(E \times EQE)^2$ versus energy as shown in Figure 12 (inset).

This plot yields an absorber layer band gap of E_g = 1.18 and 1.26 eV for −0.9 and −1.6 V, respectively.

CONCLUSION

In summary, the impact of the deposition potential, non-aqueous electrolyte, and higher working temperature on the growth and properties of CIGS layers were investigated. The growth potential was optimized by using the CV measurements on a Cu−In−Ga−Se system in ethylene glycol at a 130 °C working temperature. A wide potential window beyond −0.8 V, with respect to the Ag/AgCl reference electrode, was observed from CV measurements. XRD results revealed that the films deposited at a −0.9 V deposition potential have (112) crystal orientation, whereas the film deposited at −1.6 V shows the orientation along (220)/(204). HRTEM clearly showed the values of interplanner distances corresponding (112) and (204/220) planes. AFM confirmed the formation of globular morphology for the layers deposited at both potentials. The higher working temperature (130 °C) during the deposition leads to the formation of larger grains in as-deposited samples. The particle size was found to be increased after annealing. These larger grains are most useful for charge transport in solar cell devices. XPS confirmed the formation of Cu-rich and Cu-deficient surface of layers grown at −0.9 V and −1.6 V, respectively, which support the compositional analysis done by EDAX and XRF. The observed solar cell parameters, measured under illuminated condition of input power intensity 100 mW/cm^2 were V_{OC} = 0.357 V, J_{SC} = 27 mA/cm^2, FF = 44, and η = 4.90; and V_{OC} = 0.460 V, J_{SC} = 34 mA/cm^2, FF= 58, and η = 9.07 for the deposition potentials of −0.9 and −1.6 V, respectively. The value of shunt conductance was found to be increased and the series resistance value decreased for the solar cell prepared at −1.6 V. The film deposited at −1.6 V with (220/204) orientation showed high efficiency as compared to the film deposited at −0.9 V with a (112)-orientated film. Larger grain size correlated with the observed good performance of the solar cell made by the film deposited at higher cathodic potential. It is concluded that a solar cell device can be prepared using controlled electrodeposition parameters to obtain a (220/204) textured CIGS film with large grains which would exhibit higher efficiency.

ASSOCIATED CONTENT

Supporting Information

The Supporting Information is available free of charge on the ACS Publications website at DOI: 10.1021/acssuschemeng.7b04615.

XRF analyses of CIGS layers electrodeposited for potentials ranging from −0.8 to −1.6 V, and bulk elemental percentages composition of various CIGS samples. (PDF)

AUTHOR INFORMATION

Corresponding Author

*E-mail: n.chaure@physics.unipune.ac.in.

ORCID

Nandu B. Chaure: 0000-0002-4134-5019

Notes

The authors declare no competing financial interest.

ACKNOWLEDGMENTS

The authors are thankful to DST (SERI), DST/TM/SERI/FR/124(G), and DRDO (ERIP/ER/10003866/M/01/1388) for financial support.

REFERENCES

(1) Jackson, P.; Hariskos, D.; Wuerz, R.; Kiowski, O.; Bauer, A.; Friedlmeier, T. M.; Powalla, M. Properties of Cu(In,Ga)Se_2 solar cells with new record efficiencies up to 21.7%. *Phys. Status Solidi RRL* **2015**, *9*, 28−31.

(2) Tiwari, A. N.; Pandya, D. K.; Chopra, K. L. Fabrication and analysis of all-sprayed $CuInS_2$/ZnO solar cells. *Sol. Cells* **1987**, *22*, 263−273.

(3) Feurer, T.; Reinhard, P.; Avancini, E.; Bissig, B.; Löckinger, J.; Fuchs, P.; Carron, R.; Weiss, T. P.; Perrenoud, J.; Stutterheim, S.; Buecheler, S.; Tiwari, A. N. Progress in thin film CIGS photovoltaics − Research and development, manufacturing, and applications. *Prog. Photovoltaics* **2017**, *25*, 645−667.

(4) Green, M. A.; Hishikawa, Y.; Warta, W.; Dunlop, E. D.; Levi, D. H.; Hohl-Ebinger, J.; HO-Baillie, A. W. Y. Solar cell efficiency tables (version 50). *Prog. Photovoltaics* **2017**, *25*, 668−676.

(5) Alharbi, F. H.; Kais, S. Theoretical limits of photovoltaics efficiency and possible improvements by intuitive approaches learned from photosynthesis and quantum coherence. *Renewable Sustainable Energy Rev.* **2015**, *43*, 1073−1089.

(6) Zhang, T.; Yang, Y.; Liu, D.; Tse, S. C.; Cao, W.; Feng, Z.; Chen, S.; Qian, L. High efficiency solution-processed thin-film Cu(In,Ga)-$(Se,S)_2$ solar cells. *Energy Environ. Sci.* **2016**, *9*, 3674.

(7) Hermann, A. M.; Gonzalez, C.; Ramakrishnan, P. A.; Balzar, D.; Popa, N.; Rice, P.; Marshall, C. H.; Hilfiker, J. N.; Tiwald, T.; Sebastian, P. J.; Calixto, M. E.; Bhattacharya, R. N. Fundamental studies on large area Cu(In,Ga)Se_2 films for high efficiency solar cells. *Sol. Energy Mater. Sol. Cells* **2001**, *70*, 345−361.

(8) Abernathy, C. R.; Bates, C. W.; Anani, A. A.; Haba, B.; Smestad, G. Production of single phase chalcopyrite $CuInSe_2$ by spray pyrolysis. *Appl. Phys. Lett.* **1984**, *45*, 890−892.

(9) Rohom, A. B.; Londhe, P. U.; Chaure, N. B. Agitation dependent properties of copper indium diselenide thin films prepared by electrochemical route. *Thin Solid Films* **2016**, *615*, 366−373.

(10) Duchatelet, A.; Letty, E.; Jaime-Ferrer, S.; Grand, P. P.; Mollica, F.; Naghavi, N. The impact of reducing the thickness of electrodeposited stacked Cu/In/Ga layers on the performance of CIGS solar cells. *Sol. Energy Mater. Sol. Cells* **2017**, *162*, 114−119.

DOI: 10.1021/acssuschemeng.7b04615
ACS Sustainable Chem. Eng. XXXX, XXX, XXX−XXX

(11) Chaure, N. B.; Young, J.; Samantilleke, A. P.; Dharmadasa, I. M. Electrodeposition of n-i-p-type $CuInSe_2$ multilayers for photovoltaic application. *Sol. Energy Mater. Sol. Cells* **2004**, *81*, 125−133.
(12) Koutsikou, R.; Bouroushian, M. Pulse potential electrodeposition of (112)-textured chalcopyrite $CuInSe_2$ films from Acidic aqueous solutions. *Electrochim. Acta* **2015**, *178*, 856−870.
(13) Alcanfor, A. C.; dos Santos, L. P. M.; Dias, D. F.; Correia, A. N.; de Lima-Neto, P. Electrodeposition of indium on copper from deep eutectic solvents based on choline chloride and ethylene glycol. *Electrochim. Acta* **2017**, *235*, 553−560.
(14) Londhe, P. U.; Rohom, A. B.; Chaure, N. B. $CuInSe_2$ thin film solar cells prepared by low-cost electrodeposition techniques from a non-aqueous bath. *RSC Adv.* **2015**, *5*, 89635−89643.
(15) Londhe, P. U.; Rohom, A. B.; Lakhe, M. G.; Bhand, G. R.; Chaure, N. B. Electrochemically synthesized $CuInSe_2$ thin films from non-aqueous electrolyte for solar cell applications. *Semicond. Sci. Technol.* **2016**, *31*, 125009.
(16) Bhattacharya, R. N.; Hiltner, J. F.; Batchelor, W.; Contreras, M. A.; Noufi, R. N.; Sites, J. R. 15.4% $CuIn_{1-}xGaxSe_2$-based photovoltaic cells from solution-based precursor films. *Thin Solid Films* **2000**, *361−362*, 396−399.
(17) Chaure, N. B.; Samantilleke, A. P.; Burton, R. P.; Young, J.; Dharmadasa, I. M. Electrodeposition of p^+, p, i, n and n^+-type copper indium gallium diselenide for development of multilayer thin film solar cells. *Thin Solid Films* **2005**, *472*, 212−216.
(18) Chaure, N. B.; Bordas, S.; Samantilleke, A. P.; Chaure, S. N.; Haigh, J.; Dharmadasa, I. M. Investigation of electronic quality of chemical bath deposited cadmium sulphide layers used in thin film photovoltaic solar cells. *Thin Solid Films* **2003**, *437*, 10−17.
(19) Liao, D.; Rockett, A. Epitaxial growth of $Cu(In,Ga)Se_2$. *J. Appl. Phys.* **2002**, *91*, 1978−1983.
(20) Couzinie -Devy, F.; Barreau, N.; Kessler, J. Re-investigation of preferential orientation of $Cu(In,Ga)Se_2$ thin films grown by the three-stage process. *Prog. Photovoltaics* **2011**, *19*, 527−536.
(21) Jaffe, J.; Zunger, A. Defect-induced non polar-to-polar transition at the surface of chalcopyrite semiconductors. *Phys. Rev. B: Condens. Matter Mater. Phys.* **2001**, *64*, 241304.
(22) Schlenker, T.; Laptev, V.; Schock, H. W.; Werner, J. H. Substrate influence on $Cu(In,Ga)Se_2$ film texture. *Thin Solid Films* **2005**, *480−481*, 29−32.
(23) Contreras, M. A.; Egaas, B.; King, D.; Swartzlander, A.; Dullweber, T. Texture manipulation of $CuInSe_2$ thin films. *Thin Solid Films* **2000**, *361−362*, 167−171.
(24) Contreras, M. A.; Egaas, B.; Dippo, P. *Proc. 26th IEEE Photovoltaic Specialists' Conf.*; Anaheim, CA, IEEE, New York, 1997; p 359.
(25) Wallin, E.; Jarmar, T.; Malm, U.; Edoff, M.; Stolt, L. Influence of the average Se-to-metal overpressure during co-evaporation of $Cu(InxGa1−x)Se_2$. *Thin Solid Films* **2011**, *519*, 7237−7240.
(26) Hanna, G.; Mattheis, J.; Laptev, V.; Yamamoto, Y.; Rau, U.; Schock, H. W. Influence of the selenium flux on the growth of Cu(In,Ga)Se thin films. *Thin Solid Films* **2003**, *431−432*, 31.
(27) Contreras, M. A.; Repins, I.; Metzger, W. K.; Romero, M.; Abou-Ras, D. Se activity and its effect on $Cu(In,Ga)Se_2$ photovoltaic thin films. *Phys. Status Solidi A* **2009**, *206*, 1042.
(28) Yun, J. H.; Kim, K. H.; Ahn, B. T.; Yoon, K. H. Effect of Se beam flux rate on photovoltaic properties of CIGS cells fabricated by three-stage co-evaporation process. *Phys. Status Solidi C* **2006**, *3*, 2547.
(29) Shin, D. H.; Shin, Y. M.; Kim, J. H.; Ahn, B. T.; Yoon, K. H. Control of the Preferred Orientation of $Cu(In,Ga)Se_2$ Thin Film by the Surface Modification of Mo Film. *J. Electrochem. Soc.* **2012**, *159* (1), B1−B5.
(30) Peng, X.; Zhao, M.; Zhuang, D.; Guo, L.; Ouyang, L.; Sun, R.; Zhang, L.; Wei, Y.; Zhan, S.; Lv, X.; Wu, Y.; Ren, G. Eliminating the excess Cu_xSe phase in Cu-rich $Cu(In,Ga)Se_2$ by In_2Se_3 treatment. *J. Alloys Compd.* **2017**, *709*, 31−35.
(31) Chaisitsak, S.; Yamada, A.; Konagai, M. Preferred Orientation Control of $Cu(In_{1-x}Ga_x)Se_2$ ($x \approx 0.28$) Thin Films and Its Influence on Solar Cell Characteristics. *J. J. Appl. Phys.* **2002**, *41*, 507−513.
(32) Canava, B.; Vigneron, J.; Etcheberry, A.; Guillemoles, J. F.; Lincot, D. High resolution XPS studies of Se chemistry of a $Cu(In,Ga)Se_2$ surface. *Appl. Surf. Sci.* **2002**, *202*, 8−14.
(33) Calderon, C.; Bartolo-Perez, P.; Rodrıguez, O.; Gordillo, G. Phase identification and XPS studies of $Cu(In,Ga)Se_2$ thin films. *Microelectron. J.* **2008**, *39*, 1324−1326.
(34) Eisgruber, I. L.; Granata, J. E.; Sites, J. R.; Hou, J.; Kessler, J. Blue-photon modification of nonstandard diode barrier in $CuInSe_2$ solar cells. Sol. Energy Mater. *Sol. Energy Mater. Sol. Cells* **1998**, *53*, 367−377.
(35) Nichterwitz, M.; Caballero, R.; Kaufmann, C. A.; Schock, H. W.; Unold, T. Generation-dependent charge carrier transport in $Cu(In,Ga)Se_2$/CdS/ZnO thin-film solar-cells. *J. Appl. Phys.* **2013**, *113*, 044515.
(36) Messaoud, K. B.; Buffiere, M.; Brammertz, G.; Elanzeery, H.; Oueslati, S.; Hamon, J.; Kniknie, B. J.; Meuris, M.; Amlouk, M.; Poortmans, J. Impact of the Cd^{2+} treatment on the electrical properties of $Cu_2ZnSnSe_4$ and $Cu(In,Ga)Se_2$ solar cells. *Prog. Photovoltaics* **2015**, *23*, 1608−1620.

DOI: 10.1021/acssuschemeng.7b04615
ACS Sustainable Chem. Eng. XXXX, XXX, XXX−XXX